Liquid Crystals
Publication details, including instructions for authors and subscription information:
http://www.informaworld.com/smpp/title~content=t713926090

Numerical analysis of nematic liquid crystal alignment on asymmetric surface grating structures

Carl V. Brown; Mike J. Towler; V. C. Hui; Guy P. Bryan-Brown

Online publication date: 06 August 2010

To cite this Article Brown, Carl V. , Towler, Mike J. , Hui, V. C. and Bryan-Brown, Guy P.(2000) 'Numerical analysis of nematic liquid crystal alignment on asymmetric surface grating structures', Liquid Crystals, 27: 2, 233 — 242
To link to this Article: DOI: 10.1080/026782900203038
URL: http://dx.doi.org/10.1080/026782900203038

LIQUID CRYSTALS, 2000, VOL. 27, NO. 2, 233–242

Numerical analysis of nematic liquid crystal alignment on asymmetric surface grating structures

CARL V. BROWN†*, MIKE J. TOWLER‡, V. C. HUI
and GUY P. BRYAN-BROWN
Displays Group, DERA Malvern, Great Malvern, Worcestershire WR14 3PS, UK

(*Received 14 July 1999; accepted 27 August 1999*)

The influence of an asymmetric periodic grooved cell surface on the 2D static director configuration of a nematic liquid crystal has been investigated. The minimum in the Frank–Oseen free energy was solved numerically with the Rapini–Papoular form of the surface anchoring energy at the nematic–grating interface. Results are presented for the variation of pretilt angle in the tilted bulk director field as a function of the surface groove depth, pitch and asymmetry and the bulk parameters. The simulations demonstrate the existence of two energetically degenerate high and low pretilted bulk alignment configurations. The pretilt values in these two regimes and also for the low tilt regime with finite surface anchoring are consistent with experimental results. An effective increase in the resolution of the model is obtained by using an irregular grid to describe the surface profile.

1. Introduction

Alignment of nematic liquid crystals using a grooved surface topology is a technique which has been exploited for a number of novel device operation modes [1–5]. In these devices an electro-optical effect is originated from a voltage-induced change in the bulk liquid crystal orientation. The magnitude of this effect and the voltage at which it occurs are controlled by the exact shape of the surface topography, the elasticity of the liquid crystal medium, and the interaction energy at the nematic–substrate interface.

The basic mechanism of grating alignment was first described in terms of the elastic distortion of the nematic liquid crystal using the formalism of macroscopic continuum theory [6–8]. These models assumed that the interfacial molecules were free to reorient in the plane of the substrate. The elastic distortion energy is minimized in this case with a bulk alignment which is parallel to the groove direction. The predicted homogeneous planar alignment was realized and studied experimentally with both obliquely evaporated silicon oxide surfaces [8–10] and with photolithographic diffraction gratings [11–13].

The geometry where the liquid crystal molecular director is constrained to lie in the plane perpendicular to the direction of the grooves is of particular interest for zenithally bistable nematic devices [1, 4, 14]. These devices have potential application for low power, rugged, and flexible displays. Two possible alignment directions of interfacial molecules in this geometry are perpendicular to and parallel to the local gradient of the surface topography.

In an experimental device, perpendicular alignment is easily achieved by using a chemical surfactant, such as lecithin, which induces homeotropic alignment at the surface. The planar case is more difficult to achieve, especially for deep grooves where the elastic torque which acts to rotate the molecular director along the grooves is much larger. Two possible methods of achieving planar alignment are with another set of orthogonal grooves having a tighter pitch [15] or by using photo-induced polymer alignment in an orthogonal direction [16, 17].

In this paper an investigation of zenithal alignment of a nematic liquid crystal on an asymmetric grating surface is presented. Three different model regimes will be considered as the complexity of the description is built up in stages allowing the effects of zenithal bistability and weak surface anchoring-induced pretilt to be demonstrated. In the first regime, the liquid crystal elasticities are assumed to be infinite compared with the surface anchoring strength. The second regime takes the opposite approach with the surface anchoring energy being infinite compared with the elasticities of the liquid crystal. Finally, the third regime is when both the elasticities and the surface anchoring are finite.

* Author for correspondence; e-mail: carl.brown@eng.ox.ac.uk
† Now at: University of Oxford, Department of Engineering Science, Parks Road, Oxford OX1 3PJ, UK.
‡ Now at: Sharp Laboratories of Europe Ltd., Edmund Halley Way, Oxford Science Park, Oxford OX4 4GB, UK.

2. Theory

An asymmetric periodic 1D surface grating profile is conveniently defined by the expression in equation (1). The surface is parameterized by the peak to trough amplitude h, the period w, and the asymmetry factor A. The value of A expresses the change from a pure sinusoid at $A = 0$ to a blazed profile when $A > 0$. A realistic blazed profile without a point of inflexion is reproduced for values where $A < 0.5$. In figure (1) the surface shape shown was given by equation (1) with $A = 0.3$ and $h/w = 0.5$.

$$f(x) = \frac{h}{2} \sin\left[\frac{2\pi x}{w} + A \sin\left(\frac{2\pi x}{w}\right)\right]. \tag{1}$$

At the nematic–grating surface the free energy of the interfacial molecules is described by the well known Rapini–Papoular form of the zenithal surface anchoring energy W_S given in equation (2) [18, 19]. The angle $\theta(x)$, which is depicted in figure (1), is the tangent to the local gradient at the grating surface.

$$W_s = W_\theta \sin^2[\theta - \theta(x)]. \tag{2}$$

The bulk elastic deformation energy in the nematic liquid crystal layer is given by the Frank–Oseen free energy in equation (3) [20, 21]. The elastic constants k_{11}, k_{22} and k_{33} correspond to splay, twist and bend deformations, respectively, and the director $\mathbf{n}$ is a unit vector describing the averaged local orientation of the liquid crystal molecules.

$$2W_B = k_{11}(\nabla \quad \mathbf{n})^2 + k_{22}(\mathbf{n} \quad \nabla \times \mathbf{n})^2 + k_{33}(\mathbf{n} \times \nabla \times \mathbf{n})^2. \tag{3}$$

Variations in the orientation of the molecular director will be constrained to a 2D plane which is perpendicular to the direction of the surface grooves. The orientation at a point in space is therefore described solely by the zenithal angle $\theta(x, y)$. The director is then given by $\mathbf{n} = (\cos\theta, \sin\theta, 0)$ and the term in k_{22} disappears from equation (3). The static configuration of $\mathbf{n}$ is found by minimization of (3) which yields the Euler–Lagrange equation (4):

$$\left(\frac{\partial W_B}{\partial \theta}\right) - \nabla \quad \left(\frac{\partial W_B}{\partial \nabla \theta}\right) = 0. \tag{4}$$

For a finite surface energy, of the form shown in equation (2), the balance between the bulk nematic torque and the surface torque will be given by equation (5). Here W_B is the elastic free energy from nematic continuum theory, W_S is the surface energy; the positive sign applies at the upper surface and the negative sign applies at the lower surface of the cell.

$$\frac{\partial W_S}{\partial \theta} \pm \frac{\partial W_B}{\partial \nabla \theta} = 0. \tag{5}$$

3. Minimization of the surface energy

In this section the surface anchoring forces on an asymmetric grooved surface are considered in isolation from the liquid crystal medium. In the model geometry depicted in figure (1), the liquid crystal molecular director field is entirely oriented at an angle θ with respect to the plane of the grating. This is equivalent to a liquid crystal medium where the elastic constants are infinite.

The surface energy per unit length along the surface is given by integration of equation (2) over one period. Minimization of this energy with respect to the angle θ results in the expression in equation (6). This expresses the minimum energy pretilt angle θ_p in terms of $\theta(x)$ which is a function of the parameters h, w and A.

$$\theta_p = \frac{1}{2} \tan^{-1}\left\{\frac{\int_{x=0}^{x=w} \sin[2\theta(x)]\,dx}{\int_{x=0}^{x=w} \cos[2\theta(x)]\,dx}\right\}. \tag{6}$$

The integrals in equation (6) have been solved numerically and the predicted pretilt values are shown in figures 2(*a*) and 2(*b*) as a function of the asymmetry factor A and the ratio of the grating amplitude to the grating pitch h/w. In figure 2(*a*) the pretilt rises monotonically as a function of the asymmetry and the curves for higher values of h/w show a larger pretilt and a saturation behaviour. For a symmetrical sinusoidal grating the pretilt is zero for all values where $h/w < 0.5$.

In figure 2(*b*) the predicted pretilt is plotted as a function of h/w for different values of A. For a sinusoidal grating shape at $A = 0$ there is a sharp transition from a pretilt of 0° to a pretilt of 90° when $h/w = 0.53$. This corresponds to a transition from where planar alignment is energetically favourable in shallow grooves to where homeotropic alignment of the liquid crystal is favourable

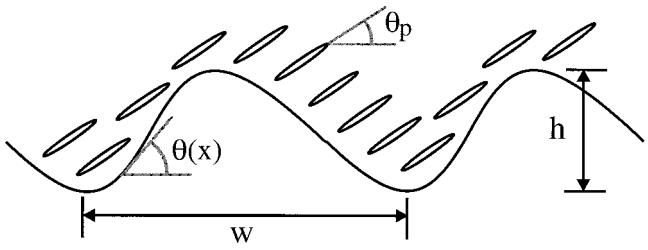

Figure 1. Depiction of the model geometry used in § 2. The liquid crystal molecular director field is aligned at a uniform zenithal angle θ above an asymmetric surface grating defined using equation (1).

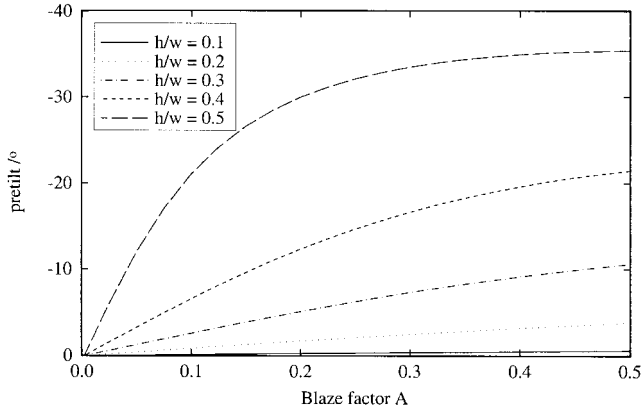

(*a*)

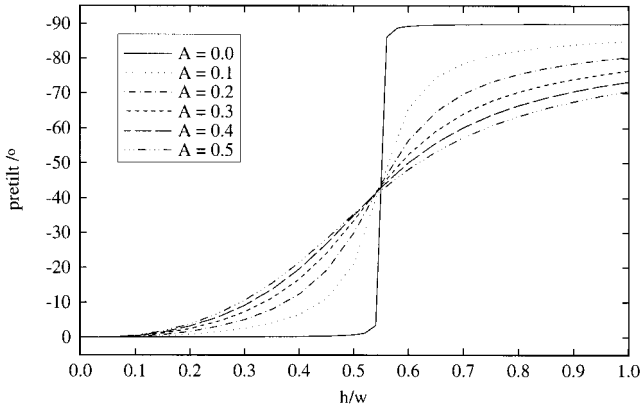

(*b*)

Figure 2. Pretilt as a function of (*a*) the asymmetry factor A and (*b*) the ratio of the grating amplitude to pitch h/w. The values were calculated using equation (3) in the model geometry shown by figure (1).

in deep grooves. As the value of A is increased the transition region becomes wider and there is a smoother variation in the pretilt from 0° to 90° as the value of h/w is increased.

This simplistic approach therefore predicts that a finite pretilt has been imparted by the asymmetry of the periodic boundary. The magnitude of this pretilt increases quickly with the asymmetry as the depth of the grooves is increased until an orientational alignment transition occurs at a threshold value of h/w. In [22, 23] a planar to homeotropic alignment transition was observed for a nematic liquid crystal on flat glass and quartz surfaces due to microscopic surface interaction effects. In this case, however, the macroscopic alignment induced by deep surface grooves or short pitch gratings was found to *suppress* the transition.

4. Calculation of bulk director configurations

The bulk elasticity of the nematic liquid crystal medium will now be taken into account in determining the alignment configuration but the surface anchoring will be assumed to be infinite. The model geometry is shown in figure (3). The liquid crystal is confined in a layer of thickness d between two identical blazed surface profiles which are arranged in an antiparallel configuration. As with the previous section a grating surface profile of amplitude h, pitch w, and asymmetry A is described by equation (1).

The director orientation is governed by equations (3) and (4). These expressions have been approximated by finite differences and solved iteratively on a rectangular mesh by a relaxation method. The grating is implemented in the model simply by truncating the rectangular mesh to give the appropriate profile $f(x)$ at the two surfaces. The director orientations at the grating surface are fixed at an angle which is parallel to the local surface gradient. These orientations are then left constant during the calculation which corresponds to the case of infinite anchoring of the interfacial molecules.

Figures 4(*a*) and 4(*b*) show two minimum energy configurations of the director field between the grating surfaces. The calculations were performed for a blazed surface grating with $A = 0.5$, $h/w = 0.6$ and with $d/w = 4.0$ and $k = k_{11} = k_{33}$. The lower half of the cell only is shown in the figures. In figure 4(*a*) the orientation of the liquid crystal follows the contours of the surface close to the lower boundary and this elastic distortion decays smoothly and exponentially through the bulk of the cell. This configuration is a singularity-free form of the solution to the continuum equation which gives a near-planar alignment regime with near zero pretilt [6].

The alignment configuration in figure 4(*b*) is characterized by structures that resemble nematic defects in

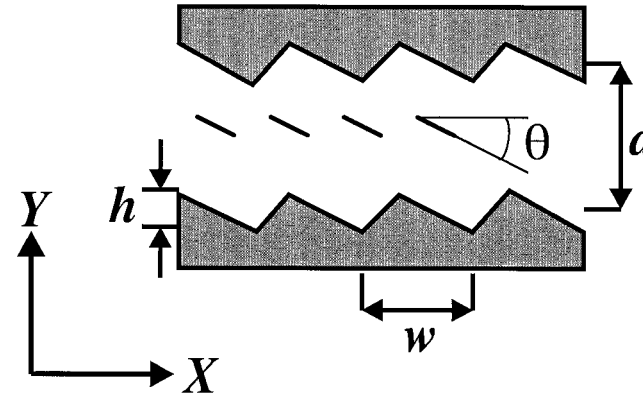

Figure 3. Depiction of the model geometry used in §2. The nematic liquid crystal is confined in a layer of thickness d between two identical blazed surface profiles which are arranged in an antiparallel configuration.

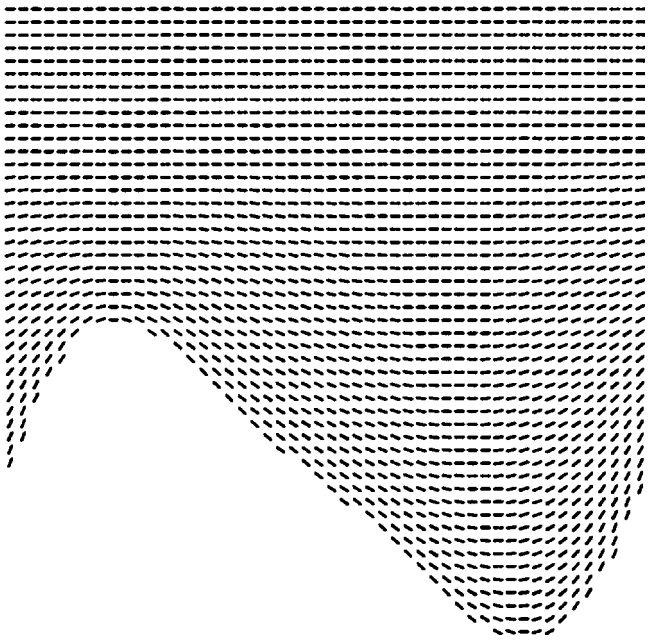

(*a*)

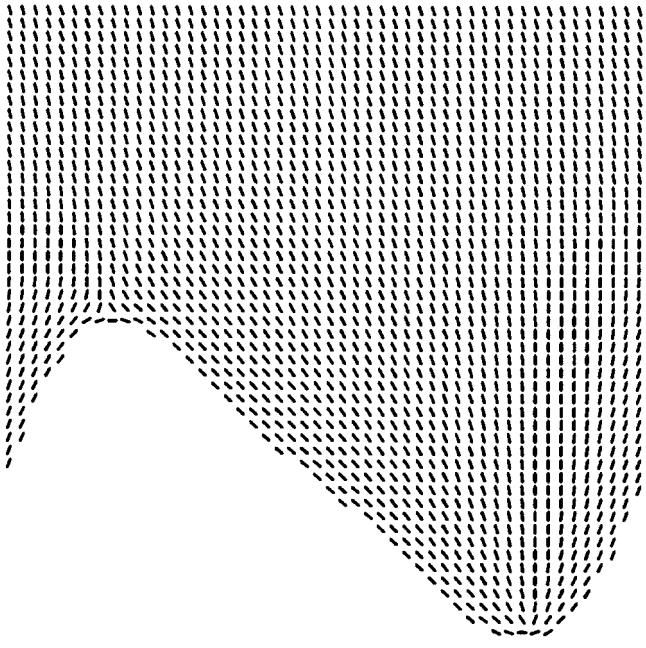

(*b*)

Figure 4. Equilibrium bulk director orientations calculated using the nematic continuum equation. A low tilt singularity-free solution is shown in (*a*) and a high pretilt defect solution is shown in (*b*) for the lower half of the cell.

the regions around the peaks and troughs in the grating surface [24, 25]. At the peak in the surface profile the orientation of the director field resembles a $-1/2$ nematic defect and at the trough in the surface the structure resembles a $+1/2$ defect. The exact position where the defect structures occur has been found to be very sensitive to the shape of the surface grating. These structures have resulted for both low and high resolution meshes and are therefore probably not simply an artefact due to the discrete nature of the model. Similar low and high pretilted alignment regimes were originally suggested by Guyon *et al.* [8] in order to explain the observed bulk orientations of thin layers of nematic liquid crystals on obliquely evaporated silicon oxide films.

For both the high and low pretilted regimes for ratios of the cell thickness to the grating period satisfying $d/w > 4.0$, the tilt in the centre of the cell varied by less than 0.1° as a function of position in the y direction. Similarly, when $d/w > 4.0$, the relative phase of the grating profiles on the upper and lower surfaces had little effect on the value of the average tilt at the centre of the cell. These observations are a consequence of the exponential decay of the distortions in the director profile with distance away from the grooved surface.

In figure (5) the total energy of low tilt singularity-free alignment configuration (filled circles) and high tilt 'defect' alignment configuration are shown as a function of the depth of the surface grooves. The energy of the low pretilt state shows a monotonic increase as h/w is increased. The rise is consistent with the prediction by Berreman for symmetric profiles [6] that the elastic distortion energy depends on the square of the grating amplitude. The energy of the high pretilt state first increases then falls roughly linearly as the grating amplitude increases. This result was independent of the resolution of the mesh used in the simulation.

The interfacial molecular director is parallel to the gradient at the surface and so for a shallow grating

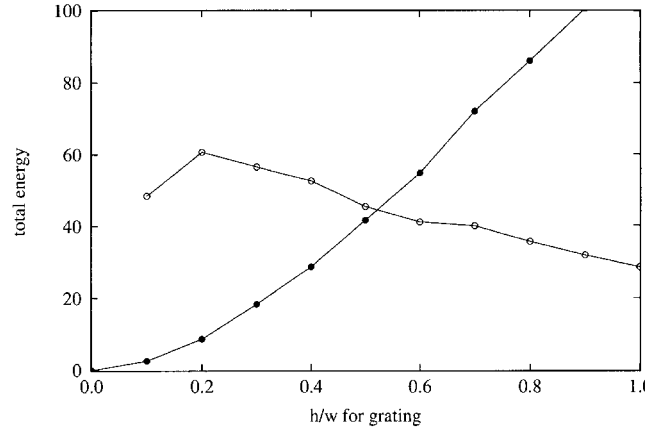

Figure 5. Integrated energy of the high and low pretilted configurations shown in figure (4) as a function of the surface groove depth. The filled circles correspond to the low tilt singularity-free configuration and the open circles to the high tilt defect configuration.

an undistorted director field with little or no pretilt is obviously more energetically favourable. There is a crossover at $h/w = 0.52$ where the energies of the high and low pretilt alignment configurations are equal and at this point zenithally bistable alignment is possible [1, 4]. It should be emphasized that the presence of real defects would cause local changes in the order parameter which have not been taken into account in the continuum description. Any quantitative prediction of the dimensions of the grating profile where bistability occurs must therefore include an offset in the energy of the high pretilt state due to the defect core energies. This may also depend to some extent on the exact surface topology.

Above the crossover the distortion energy of the low tilt alignment state increases in order to accommodate the deeper surface grooves. However, figure (6) shows that in the defect solution, the pretilt increases towards the homeotropic value in order to minimize the distortion energy as the grating amplitude increases. This is consistent with the predictions of the simple model in the previous section. The tilt in the centre of the cell in the singularity-free case remains close to zero for the values of h/w shown. The magnitude of the tilt in this alignment regime will be considered in greater detail in section (5).

5. Calculation of bulk director configurations with finite surface anchoring

The bulk alignment configuration will now be investigated with the inclusion of both the bulk elasticity of the liquid crystal and finite surface anchoring. As with the previous sections, the anchoring energy W_S is given by equation (2), the bulk elastic energy W_B by equation (3) with isotropic elastic constants $k = k_{11} = k_{33}$, and the model geometry is depicted in figure (3).

The Euler–Lagrange equation describing the bulk orientation is solved as before by approximating the derivatives of θ in x and y by first order finite differences and then using a relaxation technique to converge to a solution. The surface torque equation (5) is written in discretized form and solved simultaneously by an iterative one-step Newton method. The model was assumed to have converged to a solution when the change in θ between iterations averaged across the entire solution grid was less than 1×10^{-7} radians.

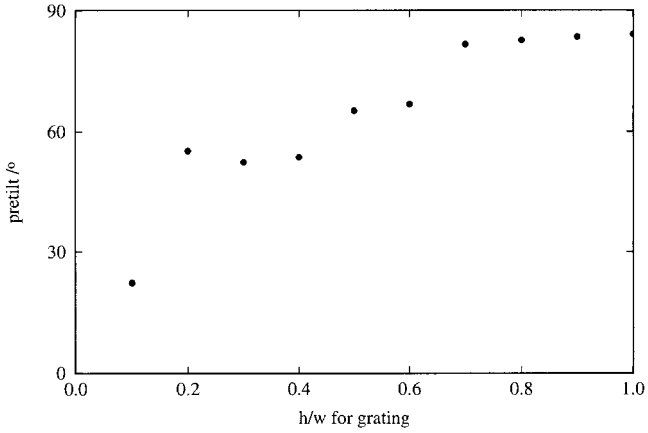

Figure 6. Tilt in the centre of the cell as a function of the groove depth in the high pretilt defect alignment configuration of figure 4 (*b*).

The strength of the surface anchoring is conveniently expressed by the dimensionless parameter $\alpha = wW_\theta/k$, where w is the pitch of the surface grating. This corresponds to a reciprocal extrapolation length scaled by a relevant grating dimension [26]. Bulk director configurations calculated using the model for the values $\alpha = 1$, 10 and 100 are shown in figure (7). The calculations were performed for a blazed surface grating with $A = 0.4$, $h/w = 0.5$ and for $d/w = 4.0$. One period of the grating surface was spanned by 50 points on the solution grid. Only the low tilt singularity-free alignment regime has been considered where the distortions in the director field follow the surface contours.

In figure 7 (*a*) the calculated director profile is shown for the case of strong anchoring where $\alpha = 100$. There is virtually no movement of the director orientation at the surface where the director angle remains close to the local surface gradient. There is a correspondingly negligible effect on the bulk director orientation which is very similar to figure 4 (*a*). For $\alpha = 10$, in figure 7 (*b*), the orientation of the director at the surface has started to pull away from the local gradient and the elastic distortion in the bulk is reduced relative to that of the previous figure. In this intermediate anchoring regime the weaker surface anchoring is beginning to influence the bulk director orientation. Figure 7 (*c*) shows the case where $\alpha = 1$, which corresponds to a weak anchoring regime. The molecular director at the surface has been pulled away from the local gradient and there is very little elastic distortion in the bulk. The net result is a director profile which is close to being uniform with a high value of the net tilt in the centre of the cell. A pretilt of this magnitude was not present for either of the more strongly anchored cases.

The averaged tilt angle in the centre of the cell is shown in figure (8) as a function of the parameter α. Several different anchoring regimes can be identified from the shape of the graph. In the region where $\alpha \geqslant 30$ the tilt is close to zero. This is effectively an infinite anchoring regime where no reorientation occurs at the surface and the bulk alignment is unaffected. The region where $5 < \alpha < 30$ is an intermediate anchoring regime where a pretilt is beginning to occur as the bulk elastic energy pulls the molecular director away at the surface. For values where $0.3 < \alpha < 3$, there is an exclusion of distortion from the bulk and a uniform tilted director

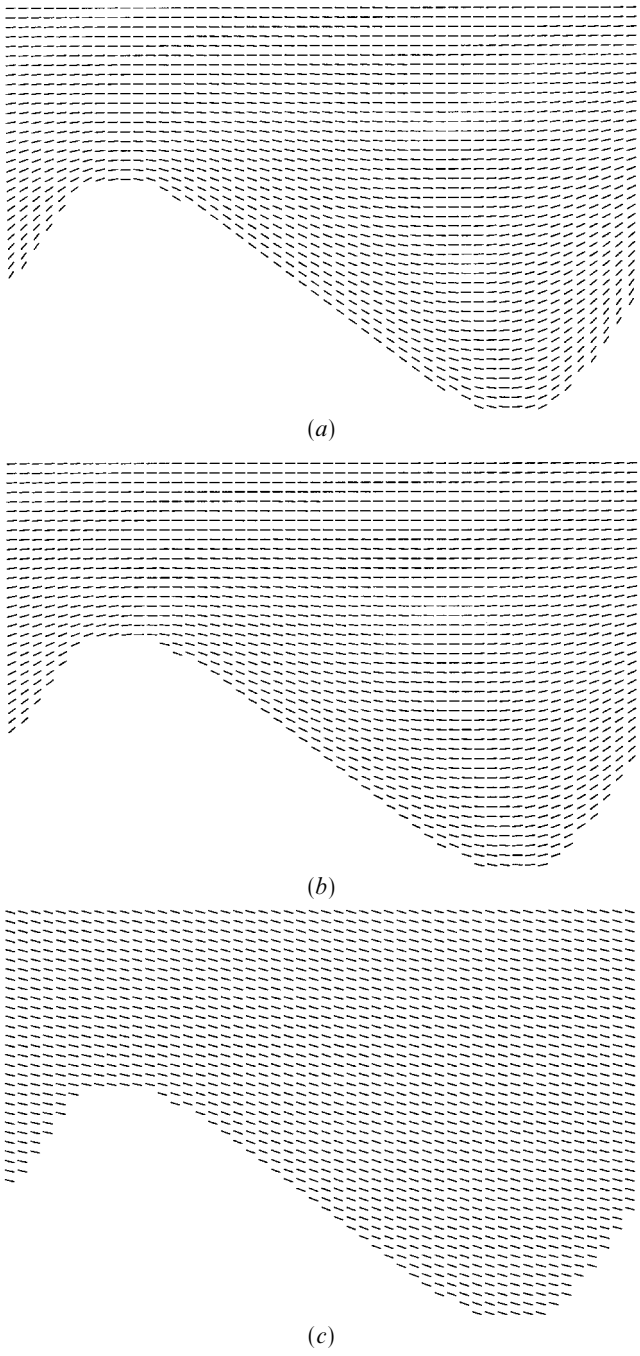

Figure 7. Equilibrium bulk director orientations calculated using the nematic continuum equation with finite surface anchoring. Director fields are shown for different values of the anchoring parameter: (*a*) $\alpha = 100$ strong anchoring, (*b*) $\alpha = 10$ intermediate anchoring regime and (*c*) $\alpha = 1$ weak anchoring.

profile results. The orientation of the molecular director at the surface is at the same tilt as the bulk and so this can be described as a weak anchoring regime.

In the case of very weak anchoring where $\alpha < 0.3$, there is insufficient coupling between the bulk director

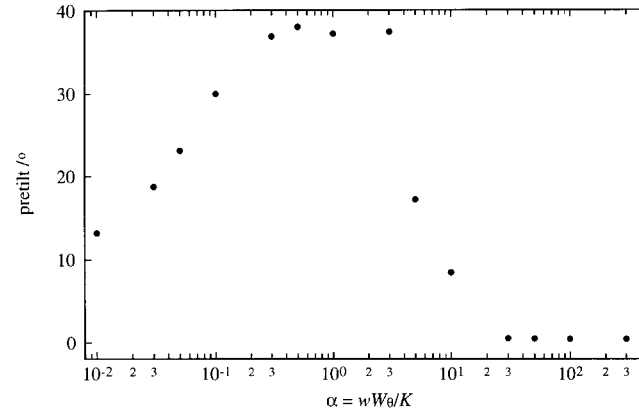

Figure 8. The averaged zenithal tilt angle in the centre of the cell as a function of the anchoring strength parameter α.

profile and the surface for the grating to have any influence. Effectively a free surface boundary condition is imposed and the bulk will assume an undistorted orientation for any given zenithal angle. A tail-off of the pretilt to a value determined solely by the average initial director configuration is therefore seen in this region in figure (8).

The value of the pretilt in the weak anchoring regime is determined by the topography of the grating surface. This corresponds to the case studied in § 2 where the elastic constants were assumed to be infinite and the pretilt was calculated by fixing the surface director orientation and minimizing the integrated value of surface energy over one grating period. For $A = 0.4$, $h/w = 0.5$, this treatment gave a pretilt of 34.7° compared with 38.0° from the finite element model in the current section.

6. Implementation of an accurate surface topology

The grating topology was originally implemented as a line on a 2D regular square lattice. The mesh size must therefore be sufficiently fine in order to reproduce the variation of the surface topography. However, there is a trade-off with the length of time required for the model to converge to a solution which increases non-linearly with the number of points on the solution grid.

In figure (9) the average tilt angle in the centre of the cell is shown as a function of d/w for the singularity-free director configuration in a cell with $A = 0.5$ and $d/w = 4.0$. The open circles show the tilt angles for a solution grid consisting of 25×100 points and the open squares are for a grid of 50×200 points. There is a large amount of scatter as the value of h/w is changed in both cases, which results because small changes in the grating amplitude are being implemented on a relatively coarse mesh.

An implementation of the surface grating which gives a more accurate definition of the topography is depicted in figure (10) for the lower surface of the cell. The points

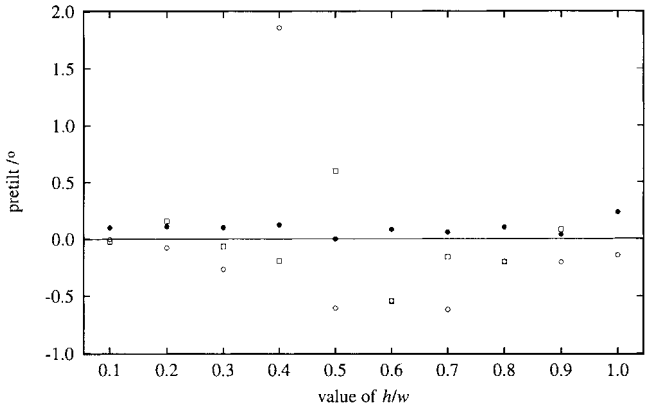

Figure 9. The average tilt angle as a function of d/w for the singularity-free director configuration with $A = 0.5$ and $d/w = 4.0$. The open symbols are for a grating defined by simple truncation of the solution grid of resolution of 25×100 points (circles) and 50×200 points (squares). The filled circles are for a grid of 25×100 points, but with a more accurate implementation of the surface topology depicted in figure (10).

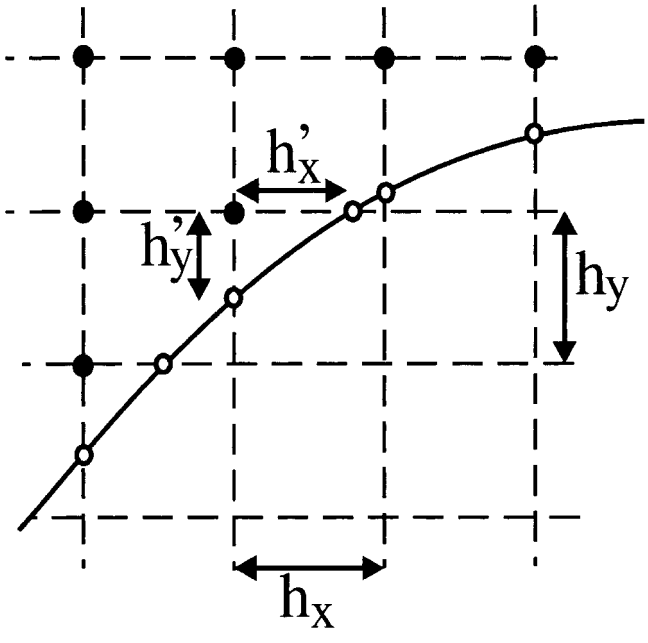

Figure 10. Implementation of the surface grating which gives a more accurate definition of the exact topography.

on the solution grid where the bulk director orientation is solved are shown by the filled circles. These points lie on a regular rectangular grid where the grid points are separated by the distance h_x in the x-direction and h_y in the y-direction. The open circles show where the surface function intersects the lines of the mesh. The discretized form of the nematic continuum equation (5) is rewritten to allow a variable step size and the values h'_x and h'_y are used in the calculation at the surface. The case of infinite surface anchoring will be considered.

Calculated director configurations are shown in figure (11) using this more accurate implementation of the surface grating. The low tilt singularity-free configuration is shown in figure 11 (*a*) and the high tilt defect solution in 11 (*b*) for blazed surface gratings with $A = 0.5$, $h/w = 0.5$ and for a cell with $d/w = 4.0$. The grating

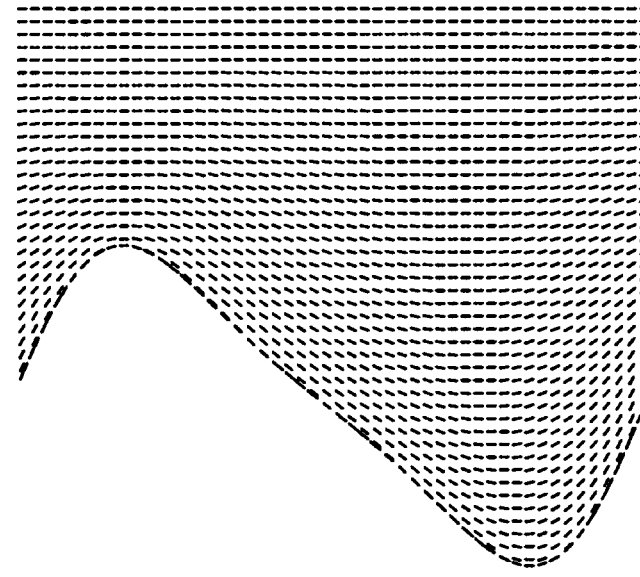

(*a*)

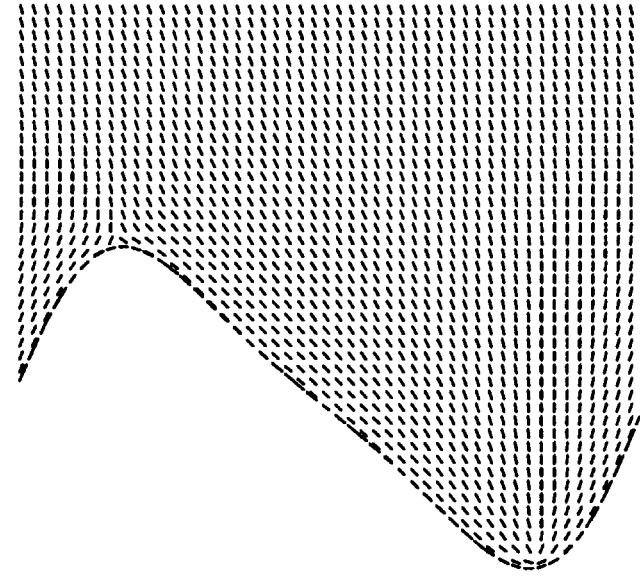

(*b*)

Figure 11. Equilibrium bulk director orientations calculated using the nematic continuum equation with a more accurate implementation of the surface topology. A low tilt singularity-free solution is shown in (*a*) and a high pretilt defect solution is shown in (*b*) for the lower half of the cell.

profile is well defined and the director orientation at points very close to the surface shows no discontinuities. Moving away from the surface, the distorted director profiles are similar to those shown in figure (4).

The advantage of the current surface implementation is demonstrated in figure (9). The filled circles show the mid-cell tilt angles for a solution grid consisting of 25×100 points. These values show less scatter than the previous results where simple truncation of the solution grid was used for both 25×100 and 50×200 points. The figure shows that for the singularity-free director configuration in a cell with $A = 0.5$ and $d/w = 4.0$, the pretilt lies in the range $0 < \theta < 0.24°$ for surface grooves of amplitude where $h/w < 1$. There is no observation of a monotonic dependence of the value of the pretilt on the amplitude of the grating as was seen in the case of weak anchoring.

7. Experimental results

A scanning electron microscope image of an experimental surface relief pattern is shown in figure (12) for a pitch of 0.84 μm and a peak to trough amplitude of 0.35 μm. The grating surface was defined in a photoresist [27] layer using hard contact photolithography. Oblique illumination was used in order to give an asymmetric structure which is highly blazed with a near vertical slope on the right hand facet. A cell was assembled from two identical grating structures in an antiparallel arrangement with a gap of 5 μm. The surfaces were treated with a chrome complex surfactant in order to give locally homeotropic alignment. The cell was filled with the nematic material E7 in the isotropic phase.

Cooling from the isotropic phase into the nematic phase gave two distinct alignment domains which were light and dark between crossed polarizers. The pretilt in the two domains was measured at 25°C using a sample rotation method [28] and a magnetic null method. The alignment in the dark state was near homeotropic with an average liquid crystal director angle of 89.7°. The light state showed a tilted homeotropic alignment with the liquid crystal director tilted at an angle of 60.5°.

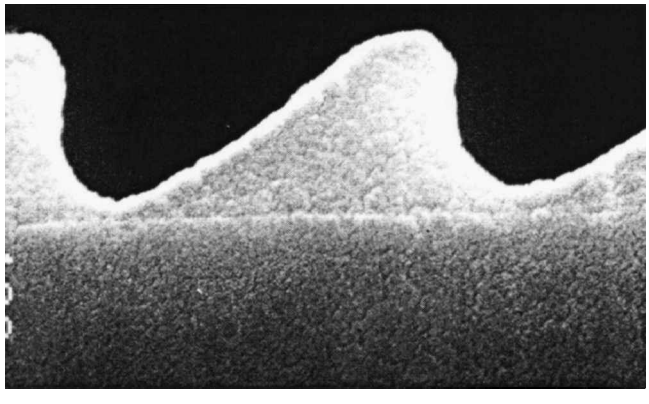

Figure 12. Picture of a fabricated surface relief pattern taken by scanning electron microscopy.

The surface relief pattern from figure (12) was digitized and implemented in the nematic continuum model using the technique described in § 5. In order to reproduce the experimental conditions at the surface, the orientation of the interfacial molecular director is locally homeotropic. Minimum energy director configurations which were calculated using the experimental cell geometry are shown in figure (13) for the lower half of the cell.

A singularity-free solution which decays to a nearly homeotropic alignment in the bulk of the cell is shown in figure 13 (*a*). The average tilt value in the centre of the cell was 92.2° for this configuration. In figure 13 (*b*) a solution is shown with defect structures in the regions of the peaks and troughs of the surface grating. This gives a tilted homeotropic director orientation in the centre of the cell with a tilt angle of 64.7°. The tilt angles in these two alignment geometries are therefore very similar to the values recorded in the experimental device. Although there is a qualitative agreement between experiment and theory, the model currently uses isotropic elastic constants $k = k_{11} = k_{33}$. In reality, for the material E7 at 25°C there is an anisotropy between the elastic constant values of magnitude $k_{33} - k_{11} = 5.2$ pN.

Experimental surfaces in figure (12) were also assembled in a cell of spacing 50 μm with the same homeotropic surfactant. This was filled with the material 8CB which has the phase sequence: crystal 21.0°C smectic A 33.5°C nematic 40.2°C isotropic liquid. A large domain of near homeotropic alignment was formed in the smectic A and nematic phases. The liquid crystal tilt angle in this domain, measured using the crystal rotation method as a function of temperature, is shown in figure (14). The circles show the pretilt on heating from the smectic A to the nematic phase and the squares show data on cooling through the phases. For both heating and cooling, the tilt angle in the smectic A phase stays roughly constant at 3.4° away from homeotropic. Below the smectic A–nematic transition temperature the value of the tilt angle drops sharply. There is a much lower pretilt in the nematic phase, for which the value is close to zero on heating.

For 8CB there is a divergence in the values of k_{11} and k_{33} on cooling in the nematic phase towards the smectic A–nematic transition temperature [29]. In the smectic A phase the bend elastic constant k_{33} is effectively infinite. This is a possible explanation for the increase in the tilt angle in the smectic A phase, because the system would be moving towards the weak anchoring regime described in § 4. The effect would be exacerbated if a grating of smaller pitch were used.

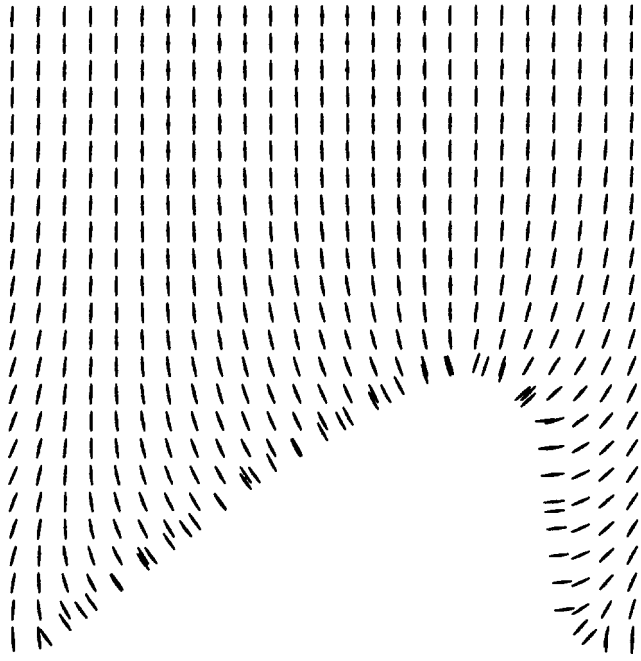

(*a*)

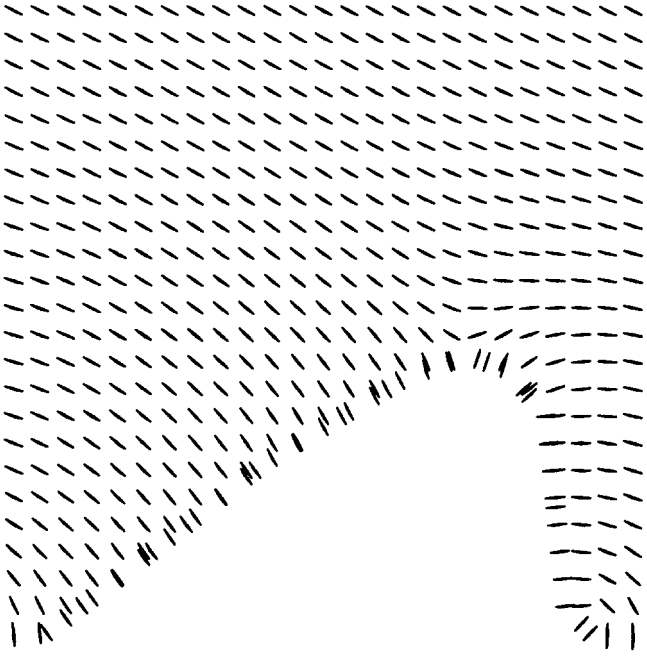

(*b*)

Figure 13. Equilibrium bulk director orientations calculated using the nematic continuum equation with the surface relief pattern shown in figure (12). A near homeotropic configuration is shown in (*a*) and a pretilted configuration in (*b*).

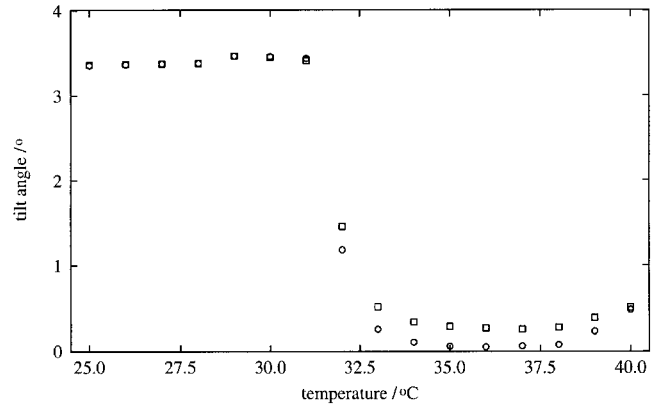

Figure 14. Experimental temperature dependence of the tilt angle for the material 8CB confined between two grating surfaces treated with a homeotropic surfactant as depicted in figure (12).

8. Conclusions

A numerical investigation of the zenithal alignment of a nematic liquid crystal on an asymmetric periodic grating surface has been presented. The complexity of the description has been built up in stages and in each of the stages alignment effects are consistently predicted which are also commensurate with observations made on experimental devices.

One of the key predictions is the existence of two distinct high and low pretilted alignment regimes and a region of bistability between the two states where they are energetically degenerate for certain values of the bulk and surface parameters. Both high and low pretilted domains are indeed observed in experimental nematic liquid crystal cells with highly blazed surfaces treated with homeotropic surfactants. Structures which resemble nematic $-1/2$ and $+1/2$ defects and lead to the highly pretilted state were reproduced in the continuum model of this geometry.

An irregular grid was used to model more accurately the surface and show that in the low tilt singularity-free alignment regime the pretilt is very close to zero. A finite pretilt was shown to appear in this regime and increase as the surface anchoring of the interfacial molecules was made weaker. However, the model has not as yet been able to reproduce the high pretilted alignment regime with weak anchoring because the numerical solution becomes unstable.

The inclusion in the model of a spatially varying nematic order parameter from Landau–de Gennes theory may allow a more detailed investigation into the stability of the defects and the total energy of the high tilt alignment configuration [26, 30].

The authors gratefully acknowledge useful discussions with Prof. F. M. Leslie (University of Strathclyde),

Prof. J. R. Sambles (Exeter University) and Prof. D. G. McDonnell O.B.E. (DERA Malvern).

References

[1] Boyd, G. D., Cheng, J., and Ngo, P. D. T., 1980, *Appl. Phys. Lett.*, **36,** 556.
[2] Thurston, R. N., Cheng, J., and Boyd, G. D., 1980, *IEEE Trans. Electron Devices*, **ED-27,** 2069.
[3] Cheng, J., Thurston, R. N., Boyd, G. D., and Meyer, R. B., 1982, *Appl. Phys. Lett.*, **40,** 1007.
[4] Bryan-Brown, G. P., Brown, C. V., Jones, J. C., Wood, E. L., Sage, I. C., Brett, P., and Rudin, J., 1997, *SID 97 Digest*, Vol. XXVIII, pp. 37–40.
[5] Bryan-Brown, G. P., Brown, C. V., Sage, I. C., and Hui, V. C., 1998, *Nature*, **392,** 365.
[6] Berreman, D. W., 1972, *Phys. Rev. Lett.*, **28,** 1683.
[7] Wolff, V., Greubel, W., and Kruger, H., 1973, *Mol. Cryst. liq. Cryst.*, **23,** 187.
[8] Guyon, E., Pieranski, P., and Boix, M., 1973, *Lett. appl. eng. Sci.*, **1,** 19.
[9] Sugimura, A., and Kawamura, T., 1984, *Jpn. J. appl. Phys.*, **23,** 137.
[10] Barberi, R., Boix, M., and Durand, G., 1989, *Appl. Phys. Lett.*, **55,** 2506.
[11] Flanders, D. C., Shaver, D. C., and Smith, H. I., 1978, *Appl. Phys. Lett.*, **32,** 597.
[12] Cheng, J., and Boyd, G. D., 1979, *Appl. Phys. Lett.*, **35,** 444.
[13] Kawata, Y., Takatoh, K., Hasegawa, M., and Sakamoto, M., 1994, *Liq. Cryst.*, **16,** 1027.
[14] Brown, C. V., Bryan-Brown, G. P., and Hui, V. C., 1997, *Mol. Cryst. liq. Cryst.*, **301,** 163.
[15] Bryan-Brown, G. P., Towler, M. J., Bancroft, M. S., and McDonnell, D. G., 1994, *SID proc. I.D.R.C.*, p. 209.
[16] Gibbons, W. M., Shannon, P. J., Sun, S. T., and Swetlin, B. J., 1991, *Nature*, **351,** 49.
[17] Schadt, M., Schmitt, K., Kozinkov, V., and Chigrinov, V., 1992, *Jpn. J. appl. Phys.*, **31,** 2155.
[18] Rapini, A., and Papoular, M., 1969, *J. Physique Colloq.*, **30,** C4-54.
[19] Barbero, G., and Durand, G., 1986, *J. Physique*, **47,** 2129.
[20] Oseen, C. W., 1933, *Trans. Faraday. Soc.*, **29,** 883; Zöcher, H., 1933, *Trans. Faraday. Soc.*, **29,** 945.
[21] Frank, F. C., 1958, *Discus. Faraday. Soc.*, **25,** 19.
[22] Känel, H. V., Litster, J. D., Melngailis, J., and Smith, H. I., 1981, *Phys. Rev. A*, **24,** 2713.
[23] Shaver, D. C., 1979, PhD thesis, Massachusetts Institute of Technology, USA.
[24] Barbero, G., 1980, *Lett Nuovo Cimento*, **29,** 553.
[25] Barbero, G., 1981, *Lett Nuovo Cimento*, **32,** 60.
[26] De Gennes, P. G., 1974, *The Physics of Liquid Crystals* (Oxford: Clarendon Press).
[27] Shipley 1805, Shipley Europe Ltd, Coventry, UK.
[28] Komitov, L., Hauck, G., and Koswig, H. D., 1984, *Cryst. Res. Technol.*, **19,** 253.
[29] Dunmur, D. A., Manterfield, M. R., Miller, W. H., and Dunleavy, J. K., 1978, *Mol. Cryst. liq. Cryst.*, **45,** 127.
[30] De Gennes, P. G., 1971, *Mol. Cryst. liq. Cryst.*, **12,** 193.